Heterobimetallic (Ferrocenyl)indenyl Rhodium Complexes. Synthesis, Crystal Structure, and Oxidative Activation of [η^5-(1-Ferrocenyl)indenyl]RhL_2 [L_2 = COD, NBD, $(CO)_2$][||]

Saverio Santi,*[,†] Alberto Ceccon,*[,†] Laura Crociani,[†] Alessandro Gambaro,[†] Paolo Ganis,[†] Mauro Tiso,[†] Alfonso Venzo,[‡] and Alessia Bacchi[§]

Dipartimento di Chimica Fisica, Università degli Studi di Padova, Via Loredan 2, 35131 Padova, Italy, CNR, Centro di Studio Sugli Stati Molecolari Radicalici ed Eccitati, Via Loredan 2, 35131 Padova, Italy, and Dipartimento di Chimica Generale ed Inorganica, Chimica Analitica, Chimica Fisica, Università degli Studi di Parma, Parco Area delle Scienze 17/A, 43100 Parma, Italy

Received July 10, 2001

The binuclear [η^5-(1-ferrocenyl)indenyl]Rh(NBD) (**1**), [η^5-(1-ferrocenyl)indenyl]Rh(COD) (**1a**), and [η^5-(1-ferrocenyl)indenyl]Rh$(CO)_2$ (**2**) complexes have been synthesized (NBD = norbornadiene; COD = cycloocta-1,5-diene). The crystal structure determination showed that the iron and rhodium nuclei are disposed in a *transoid* configuration in **1** probably to avoid steric repulsions. On the contrary, in **2** the metals are in a *cisoid* configuration due to the presence of stabilizing π-hydrogen bonds between the CO's and the hydrogens of the unsubstituted cyclopentadienyl ring. The results of the chemical and electrochemical oxidation of **2** are in favor of the existence of an effective interaction between the two metals.

Introduction

Much of the interest about the construction of model compounds suitable for investigating the phenomena associated with the interactions between two or more metal centers, the so-called *cooperative effect*, has been concentrated on homobimetallic complexes and in particular on bis-iron compounds.[1] This may be ascribed mainly to the chemical stability of neutral ferrocenes and their oxidized species and to the relatively simple synthetic procedure of generating the complexes.

Despite their intrinsic interest, less attention has been paid to those complexes having two different metal units anchored in close proximity. This reflects mainly the difficulty in synthesizing such complexes. In fact, while the simultaneous introduction of two different metals in bis-cyclopentadienyl ligands has been rarely achieved without much complication, only in a few cases the two-step pathway consisting of metalation of one of the two Cp rings leaving the second one free for further metalation has been possible. In most cases, the synthesized heterobimetallic complexes contain two metal units separated by a saturated or an unsaturated chain.[2] On the other hand, heteronuclear complexes with two Cp rings directly connected by a σ bond (*fulvalene bridge*) are quite limited and often contain a ferrocenyl moiety linked to different metallocene groups.[3]

There are severe reasons to be interested in the synthesis and characterization of heterobimetallic complexes containing one ferrocenyl portion bonded to a $CpML_n$ group (nonmetallocene complexes). These reasons include (i) the easy oxidation of the ferrocene unit; (ii) the chemical stability of the neutral ferrocenyl moiety as well as its oxidized species; (iii) the strong coupling between metal centers linked by a fulvalene bridge; and (iv) the great variety of ancillary ligands, L, which can modulate the electron density at the M nucleus by varying its physical and chemical properties.

A few years ago, the synthesis and properties of a number of ferrocenyl-based fulvalene-bridged heterobimetallic complexes containing the (η-C_3R_4)-M$(CO)_2$ fragment (M = Mo, W; R = H, Ph) together with their electrochemical behavior were reported.[4] The two-step synthesis was based on the preparation and isolation of the ferrocenyl-substituted cyclopentadiene ligand,

[||] Presented at the 2001 Joint International Meeting: 200th Meeting of Electrochemical Society and 52th Meeting of the International Society of Electrochemistry, San Francisco, September 2−7, 2001.

* Corresponding author. E-mail: s.santi@chfi.unipd.it.
[†] Università degli Studi di Padova.
[‡] CNR, Centro di Studio Sugli Stati Molecolari Radicalici ed Eccitati.
[§] Università degli Studi di Parma.

(1) (a) Marks, T. J. *Acc. Chem. Res.* **1992**, *25*, 57. (b) Süss-Fink, G.; Meister, G. *Adv. Organomet. Chem.* **1993**, *35*, 41. (c) Ward, M. D. *Chem. Soc. Rev.* **1995**, 121. (d) Beck, W.; Niemer, B.; Wieser, M. *Angew. Chem., Int. Ed. Engl.* **1993**, *32*, 923. (e) Lang, H. *Angew. Chem., Int. Ed. Engl.* **1994**, *33*, 547. (f) Bunz, V. *Angew. Chem., Int. Ed. Engl.* **1996**, *35*, 969. (g) Barlow, S.; O'Hare, D. *Chem. Rev.* **1997**, 6377. (h) McCleverty, J. A.; Ward, M. D. *Acc. Chem. Res.* **1998**, *31*, 842.

(2) (a) Bitterwolf, T. E. *J. Organomet. Chem.* **1986**, *312*, 197. (b) McGovern, P. A.; Volhardt, K. P. C. *Synlett* **1990**, 493. (c) Hudezceck, A.; Köhler, F. H. *Organometallics* **1992**, *11*, 1773. (d) Astruc, D. *Acc. Chem. Res.* **1997**, *30*, 383. (e) Werner, H. *Inorg. Chim. Acta* **1992**, *198*, 715. (f) Nakashima, S.; Hori, A.; Watanabe, M.; Motoyama, I. *J. Organomet. Chem.* **1997**, *542*, 271. (g) Dong, T. Y.; Lee, S. H.; Chang, C. K.; Lin, H. H.; Lin, K. J. *Organometallics* **1997**, *16*, 2773. (h) Boese, R.; Cammack, J. K.; Hatzger, A. J.; Pflug, K.; Tolman, W. B.; Volhardt, P. C.; Weidman, T. W. *J. Am. Chem. Soc.* **1997**, *119*, 6757.

(3) Lee, S. G.; Lee, S. S.; Chung, Y. K. *Inorg. Chim. Acta* **1999**, *286*, 215.

(4) (a) Wan, S.; Begley, M. G.; Montford, P. *Inorg. Chim. Acta* **1995**, *489*, C28−C31. (b) Begley, M. G.; Montford, P.; Stewart, P. J.; Swallow, D.; Wan, S. *J. Chem. Soc., Dalton Trans.* **1996**, 1323.

10.1021/om010621g CCC: $22.00
Publication on Web 01/08/2002

which was subsequently deprotonated and metalated with the appropriate metal complex. The overall yield was modest, although the use of the $[C_5H_5FeC_5H_4]^-Li^+$ salt as reagent to prepare heterobimetallic fulvalenyl derivatives may be convenient since its isolation in gram quantities is possible.

As a part of our continuing program to expand the chemistry of heterobimetallic indenyl complexes,[5] we have initiated a study on [η^5-(1-ferrocenyl)indenyl]RhL_2 complexes in anticipation that the close proximity of an iron unit (and of its oxidized species) to a rhodium center associated with the coordinative flexibility of the indenyl ligand will result in unusual structural and chemical properties.

Here we report the first synthesis and the results of structural and voltammetric behavior of some of these iron−rhodium complexes. The knowledge of their crystal structures allows the comparison with the structure of the mononuclear (3-ferrocenyl)indene (**3**).

Experimental Section

General Procedures. All reactions and complex manipulations were performed in an oxygen- and moisture-free atmosphere; *n*-pentane was deoxygenated before use. THF (Acros) was purified by distillation from Na/benzophenone under argon atmosphere, and then deoxygenated with vacuum line techniques just before use. Ferrocene (Acros) was purified by crystallization before use. (3-Ferrocenyl)indene (**3**) was synthesized according to the literature.[3] Crystals suitable for X-ray analysis were grown from *n*-pentane solutions at −50 °C. Microanalyses were performed at the Dipartimento di Chimica Inorganica, Metallorganica ed Analitica, Università di Padova. IR spectra were recorded on a Bruker Equinox 55 FT-IR spectrometer. ^{1}H and ^{13}C NMR spectra were obtained as acetone-d_6 solutions on a Bruker Avance-400 spectrometer operating at 400.13 and 100.61 MHz, respectively. The assignments of the proton resonances were performed by standard chemical shift correlations and NOESY experiments. The ^{13}C resonances were attributed through 2D-heterocorrelated COSY experiments (HMQC with *bird* sequence[6] and quadrature along F1 achieved using the TPPI method[7] for the H-bonded carbon atoms, HMBC[8] for the quaternary ones). Cyclic voltammetry experiments were performed in an airtight three-electrode cell connected to a vacuum/argon line. The reference electrode was a SCE (Tacussel ECS C10) separated from the solution by a bridge compartment filled with the same solvent/supporting electrolyte solution used in the cell. The counter electrode was a platinum spiral with ca. 1 cm^2 apparent surface area. The working electrodes were disks obtained from cross section of gold wires of different diameters (0.5, 0.125, and 0.025 mm) sealed in glass. Between each CV scan the working electrodes were polished on alumina according to standard procedures and sonicated before use. An EG&G PAR-175 signal generator was used. The currents and potentials were recorded on a Lecroy 9310L oscilloscope. The potentiostat was home-built with a positive feedback loop for compensation of ohmic drop.[9]

[η^5-(1-Ferrocenyl)indenyl]Rh(NBD) (1). *n*-Butyllithium (0.4 mmol, 0.25 mL of a 1.6 M solution in hexanes) was added dropwise to a stirring solution of (3-ferrocenyl)indene (120 mg, 0.4 mmol) in THF (25 mL) at −78 °C. The orange solution turned immediately to red. After 30 min solid [Rh(μ-Cl)(NBD)]$_2$[10a] (138 mg, 0.6 mmol) was added, and the solution was stirred for 90 min while the temperature was raised slowly up to room temperature. The solvent was removed under vacuum, and the residue was treated with cyclohexane (50 mL). After filtration of the mixture the solution was concentrated and chromatographed on a short column of activated basic Al_2O_3 eluting with a mixture of petroleum ether (80%) and Et_2O (20%), yielding upon removal of the solvent 172 mg (87%) of the product as an orange microcrystalline powder. Crystals suitable for X-ray analysis were grown from *n*-pentane solutions at −50 °C. Mp: 121 °C. Anal. Calcd for $C_{26}H_{23}FeRh$: C, 63.18; H, 4.70. Found: C, 62.96; H, 4.62. ^{1}H NMR (CD_3COCD_3, ν_o 400.13 MHz, ppm from internal Me_4Si; for atom labeling see below): δ 7.838 (m, 1H, H7), 7.320 (m, 1H, H4), 7.168 (m, 1H, H6), 7.068 (m, 1H, H5), 6.354 (dd, 1H, ^3J(H2,H3) 2.8 Hz, J(^{103}Rh,H2) 2.0 Hz, H2), 5.151 (d, 1H, ^3J(H2,H3) 2.8 Hz, H3), 4.453 (m, 1H, Hα'), 4.512 (m, 1H, Hα), 4.217 (m, 1H, Hβ), 4.223 (m, 1H, Hβ'), and 4.079 (s, 5H, C_5H_5 ring). ^{13}C{^{1}H} NMR (CD_3COCD_3, ν_o 400.13 MHz, ppm from internal Me_4Si): δ 122.7 (C6), 122.6 (C5), 120.7 (C4), 120.2 (C7) 112.1 (^1J(^{103}Rh−^{13}C) <1 Hz, C7a), 109.4 (^1J(^{103}Rh−^{13}C) 2.5 Hz, C3a), 92.20 (^1J(^{103}Rh−^{13}C) 5.4 Hz, C2), 89.20 (^1J(^{103}Rh−^{13}C) 3.5 Hz, C1), 73.03 (^1J(^{103}Rh−^{13}C) 5.4 Hz, C3), 70.1 (^2J(^{103}Rh−^{13}C) 1.5 Hz, C*j*), 69.71 (C_5H_5), 68.80 (Cβ), 67.86 (Cβ'), 67.285 (Cα), 67.282 (Cα'), 58.27 (^1J(^{103}Rh−^{13}C) 6.9 Hz, NBD CH_2 carbon), 47.93 (^1J(^{103}Rh−^{13}C) 2.6 Hz, NBD bridgehead carbons), 41.14 and 38.84 (^1J(^{103}Rh−^{13}C) 10.4 and 10.4 Hz, NBD olefin carbons).

[η^5-(1-Ferrocenyl)indenyl]Rh(COD) (1a). *n*-Butyllithium (0.4 mmol, 0.25 mL of a 1.6 M solution in hexanes) was added dropwise to a stirring solution of (3-ferrocenyl)indene (120 mg, 0.4 mmol) in THF (25 mL) at −78 °C. The orange solution turned immediately to red. After 30 min [Rh(μ-Cl)(COD)]$_2$[10b] (148 mg, 0.6 mmol) was added, and the solution was stirred for 45 min while the temperature was raised slowly up to room temperature. The solvent was removed under vacuum, and the residue was treated with cyclohexane (50 mL). After filtration of the mixture the solution was concentrated and chromatographed on a short column of activated basic Al_2O_3 eluting with a mixture of petroleum ether (80%) and Et_2O (20%), yielding, upon removal of the solvent, 136 mg (80%) of the product as an orange microcrystalline powder. Mp: 141−142 °C. Anal. Calcd for $C_{27}H_{27}FeRh$: C, 63.55; H, 5.33. Found: C, 63.42; H, 5.44. ^{1}H NMR (CD_3COCD_3, ν_o 400.13 MHz, ppm from internal Me_4Si): δ 7.753 (m, 1H, H7), 7.274, 1H, H4), 7.168 (m, 1H, H6), 7.107 (m, 1H, H5), 6.328 (dd, 1H, ^3J(H2,H3) 2.8 Hz, J(^{103}Rh,H2) 1.95 Hz, H2), 5.146 (d, 1H, ^3J(H2,H3) 2.9 Hz, H3), 4.557 (m, 1H, Hα), 4.537 (m, 1H, Hα'), 4.229 (m, 1H, Hβ), 4.226 (m, 1H, Hβ'), 4.024 (s, 5H, C_5H_5 ring), 3.746 and 3.266 (2 m, 2H each, COD olefin protons), 1.785 and 1.716 (2 m, 4 H each, COD methylene protons). ^{13}C{^{1}H} NMR (CD_3COCD_3, ν_o 400.13 MHz, ppm from internal Me_4Si): δ 123.20 (C6), 123.13 (C5), 120.7 (C4), 120.1 (C7) 113.7 (^1J(^{103}Rh−^{13}C) 1.9 Hz, C3a), 111.6

(5) Bonifaci, C.; Ceccon, A.; Gambaro, A.; Manoli, F.; Mantovani, L.; Ganis, P.; Santi, S.; Venzo, A. *J. Organomet. Chem.* **1998**, *557*, 97. (b) Cecchetto, P.; Ceccon, A.; Gambaro, A.; Santi, S.; Ganis, P.; Gobetto, R.; Valle, G.; Venzo, A. *Organometallics* **1998**, *17*, 752. (c) Mantovani, L.; Ceccon, A.; Gambaro, A.; Santi, S.; Ganis, P.; Venzo, A. *Organometallics* **1997**, *16*, 2682. (d) Bonifaci, C.; Carta, G.; Ceccon, A.; Gambaro, A.; Santi, S.; Venzo, A. *Organometallics* **1996**, *15*, 1630. (e) Bonifaci, C.; Ceccon, A.; Gambaro, A.; Ganis, P.; Santi, S.; Valle, G.; Venzo, A. *J. Organomet. Chem.* **1995**, *492*, 35. (f) Bonifaci, C.; Ceccon, A.; Gambaro, A.; Ganis, P.; Santi, S.; Venzo, A. *Organometallics* **1995**, *14*, 2430. (g) Bonifici C.; Ceccon, A.; Gambaro, A.; Ganis, P.; Mantovani, L.; Santi, S.; Venzo, A. *J. Organomet. Chem.* **1994**, *474*, 267. (h) Bonifaci, C.; Ceccon, A.; Gambaro, A.; Ganis, P.; Santi, S.; Valle, G.; Venzo, A. *Organometallics* **1993**, *12*, 4211. (i) Ceccon, A.; Elsevier: C. J.; Ernsting, J. M.; Gambaro, A.; Santi, S.; Venzo, A. *Inorg. Chim. Acta* **1993**, *104*, 15. (j) Ceccon, A.; Gambaro, A.; Santi, S.; Venzo, A. *J. Mol. Catal.* **1991**, *69*, L1−L6. (k) Ceccon, A.; Gambaro, A.; Santi, S.; Valle, G.; Venzo, A. *J. Chem. Soc., Chem. Commun.* **1989**, 51.

(6) Bax, A.; Subramanian, S. *J. Magn. Reson.* **1986**, *67*, 565.

(7) (a) Otting, G.; Wüthrich, K. *J. Magn. Reson.* **1988**, *67*, 569. (b) Drobny, G.; Pines, A.; Sinton, S.; Weitekamp, D.; Wemmer, D. *Faraday Symp. Chem. Soc.* **1979**, *13*, 49.

(8) Bax, A.; Summers, M. F. *J. Am. Chem. Soc.* **1986**, *108*, 2093.

(9) Amatore, C.; Lefrou, C.; Pflüger, F. *J. Electroanal. Chem.* **1989**, *43*, 270.

(10) (a) Abel, E. W.; Bennet, M. A.; Wilkinson, G. *J. Chem. Soc.* **1959**, 3178. (b) Chatt, J.; Venanzi, M. L. *J. Chem. Soc.* **1957**, 4735.

Table 1. Summary of Crystal Data and Intensity Data Collection for 1, 2, and 3

	1	2	3
formula	$C_{26}H_{23}FeRh$	$C_{21}H_{15}FeO_2Rh$	$C_{19}H_{16}Fe$
molecular weight	494.22	458.10	300.18
cryst syst	monoclinic	monoclinic	orthorhombic
space group	$P2_1/a$	$P2_1/c$	$Pcab$
a/Å	10.779(2)	15.137(5)	18.245(5)
b/Å	9.982(2)	11.129(5)	19.423(5)
c/Å	18.309(2)	10.528(5)	8.029(3)
β/deg	93.19(2)	73.79(3)	
V/Å^3	1966.9(8)	1703.0(12)	2845.3(15)
Z	4	4	8
cryst dimens/mm	0.4 × 0.3 × 0.2	0.4 × 0.4 × 0.2	0.4 × 0.3 × 0.2
D_c/g cm^{-3}	1.669	1.787	1.401
μ/cm^{-1}	1.585	1.831	1.050
T/K	293	293	293
radiation	graphite-monochromated Mo Kα (λ = 0.71069 Å)		
θ range for data collection/deg	$2.23 \le \theta \le 26.08$	$1.40 \le \theta \le 26.58$	$3.06 \le \theta \le 26.01$
no. of obsd reflns (ind)	6336 (6336)	9452 (3516)	5469 (2787)
R(obsd data/all data)	0.039/0.048	0.024/0.031	0.032/0.132
R_w(obsd data/all data)	0.120/0.127	0.063/0.068	0.057/0.078
largest ΔF, e Å^3	0.714	0.883	0.274
GOF	1.132	1.025	0.773

($^1J(^{103}Rh-^{13}C)$ 1.9 Hz, C7a), 92.59 ($^1J(^{103}Rh-^{13}C)$ 5.3 Hz, C2), 81.60 ($^1J(^{103}Rh-^{13}C)$ 1.9 Hz, C1), 75.28 ($^1J(^{103}Rh-^{13}C)$ 4.6 Hz, C3), 69.79 (C_5H_5), 69.13 (Cβ'), 68.13 (Cβ), 67.37 ($^2J(^{103}Rh-^{13}C)$ 1.9 Hz, Cj), 67.16 (Cα), 66.88 (Cα′), 72.17 and 68.58 ($^1J(^{103}Rh-^{13}C)$ 14.6 and 13.8 Hz, COD olefin carbons), 31.94 and 31.72 (COD methylene carbons).

[η^5-(1-Ferrocenyl)indenyl]Rh(CO)$_2$ (2). A slurry of complex **1** (200 mg, 0.4 mmol) in *n*-pentane (100 mL) was bubbled with CO for 3 h at room temperature. The orange solution was then concentrated to ca. 2 mL by bubbling it with CO and argon, and the supernatant liquid was removed, leaving an orange powder which was washed twice with 1 mL of cool *n*-pentane. The powder was dried at 45 °C under a stream of argon to afford 121 mg (65% yield) of **2**. Crystals suitable for X-ray analysis were grown from *n*-pentane solutions at −50 °C. Mp: dec 90 °C. Anal. Calcd for $C_{21}H_{15}FeO_2Rh$: C, 55.06; H, 3.30. Found: C, 55.17; H, 3.26. IR (CH_2Cl_2): ν(CO) 2037(s) and 1979(s) cm^{-1}. ^{1}H NMR (CD_3COCD_3, ν_o 400.13 MHz, ppm from internal Me_4Si): δ 7.836 (m, 1H, H7), 7.39 (m, 1H, H4), 7.301 (m, 1H, H6), 7.206 (m, 1H, H5), 6.535 (dd, 1H, ^3J(H2,H3) 2.9 Hz, $J(^{103}Rh,H2)$ 2.6 Hz, H2), 5.146 (d, 1H, ^3J(H2,H3) 2.9 Hz, H3), 4.778 (m, 1H, Hα′), 4.722 (m, 1H, Hα), 4.390 (m, 1H, Hβ), 4.380 (m, 1H, Hβ'), and 4.165 (s, 5H, C_5H_5 ring). ^{13}C{^{1}H} NMR (CD_3COCD_3, ν_o 400.13 MHz, ppm from internal Me_4Si): δ 190.40 ($^1J(^{103}Rh-^{13}C)$ 87 Hz, CO), 124.8 (C6), 124.7 (C5), 119.3 (C4), 118.7 (C7) 116.6 ($^1J(^{103}Rh-^{13}C)$ 2.1 Hz, C3a), 116.2 ($^1J(^{103}Rh-^{13}C)$ 1.6 Hz, C7a), 97.33 ($^1J(^{103}Rh-^{13}C)$ 6.3 Hz, C2), 97.11 ($^1J(^{103}Rh-^{13}C)$ 3.2 Hz, C1), 79.52 ($^2J(^{103}Rh-^{13}C)$ ca. 1 Hz, Cj), 72.61 ($^1J(^{103}Rh-^{13}C)$ 3.9 Hz, C3), 69.33 (C_5H_5), 69.08 (Cα′), 68.70 (Cβ), 68.08 (Cβ'), and 67.94 (Cα).

Oxidation of 2 with *p*-Benzoquinone. To a stirring solution of **2** (66 mg, 0.14 mmol) in THF (3 mL) was added a solution of *p*-benzoquinone (16 mg, 0.14 mmol) and NH_4PF_6 (45.6 mg, 0.28 mmol) in THF (5 mL) at room temperature. After 19 h the solvent was removed under vacuum; the residue was washed with *n*-hexane (2 × 10 mL), dissolved in the minimum amount of CH_2Cl_2, and then filtered. Addition of *n*-hexane (20 mL) yielded a brown powder. IR (CH_2Cl_2): ν(CO) 2097(s) and 2022(s) cm^{-1}. ^{1}H NMR (CD_3COCD_3, ν_o 400.13 MHz, ppm from internal Me_4Si): δ 7.90 (m, 1H, H7), 7.41 (m, 1H, H4), 7.52 (m, 1H, H6), 7.46 (m, 1H, H5), 6.32 (d, 1H, ^3J(H2,H3) 2.8 Hz, H3), 6.24 (dd, 1H, ^3J(H2,H3) 2.8 Hz, $J(^{103}Rh,H2)$ 1.7 Hz, H2), 4.92 (m, 1H, Hα), 4.76 (m, 1H, Hα′), 4.49 (m, 1H, Hβ'), 4.480 (m, 1H, Hβ), and 4.18 (s, 5H, C_5H_5 ring). ^{13}C{^{1}H} NMR (CD_3COCD_3, ν_o 400.13 MHz, ppm from internal Me_4Si): δ 174.60 ($^1J(^{103}Rh-^{13}C)$ 88 Hz, CO), 128.72 (C6), 128.70 (C5), 122.5 (C4), 121.4 (C7), 107.00 ($^1J(^{103}Rh-^{13}C)$ 6.1 Hz, C3a), 105.59 ($^1J(^{103}Rh-^{13}C)$ 3.7 Hz, C7a), 98.96 ($^1J(^{103}Rh-^{13}C)$ 3.2 Hz, C1), 89.59 ($^1J(^{103}Rh-^{13}C)$ 7.7 Hz, C2), 80.85 ($^2J(^{103}Rh-^{13}C)$ ca. 1 Hz, Cj), 77.02 ($^1J(^{103}Rh-^{13}C)$ 3.9 Hz, C3), 70.42 (Cβ), 69.99 (C_5H_5), 69.68 (Cβ'), 69.30 (Cα′), and 69.13 (Cα).

Table 2. Selected Bond Distances, Nonbonded Distances, and Torsion Angles for the Complexes 1, 2, and 3

	1	2	3
Bond Distances/Å			
C6−C10	1.431(7)	1.486(3)	1.467(4)
C8−C9	1.423(8)	1.459(4)	1.489(5)
C6−C7	1.412(7)	1.409(4)	1.384(4)
C7−C8	1.402(7)	1.413(4)	1.480(6)
C4−C6	1.474(8)	1.471(4)	1.472(4)
average C−C in the C_5H_5 ring	1.400(9)	1.408(5)	1.403(6)
average C−C in the Ph ring	1.399(8)	1.392(4)	1.385(5)
average Fe−C	2.040(6)	2.038(3)	2.026(4)
Rh−C10	2.315(6)	2.382(3)	
Rh−C9	2.337(5)	2.364(3)	
Rh−C8	2.211(5)	2.206(3)	
Rh−C7	2.247(5)	2.254(3)	
Rh−C6	2.253(5)	2.246(3)	
Nonbonded Distances/Å			
H7···H15		3.10	
H7···H19		2.97	
H15···H21		2.84	
H16···O2		2.95	
H11···H19			3.16
H11···H15			3.05
Bond and Torsion Angles/deg.			
C20−Rh−C21		91.0(3)	
C3−C4−C6−C10	27.0	−52.7	25.2

Crystallography. Crystal data, intensity data collection, and processing details of **1**−**3** are reported in Table 1. Selected bond lengths and angles are presented in Table 2. X-ray diffraction data were collected on a Philips PW1100 diffractometer equipped with a scintillation counter for compounds **1** and **3** and on a Bruker-Siemens SMART AXS 1000 equipped with CCD detector for **2**, both using graphite-monochromated Mo Kα radiation (λ = 0.71069 Å). Data were corrected for absorption effects by the ψ-scan method[11] for **1** and by the SADABS[12] procedure for **2**. Both structures were solved by direct methods[13] and refined by full matrix least squares on

(11) North, A. C. T.; Phillips, D. C.; Mathews, F. S. *Acta Crystallogr.* **1968**, *A24*, 351−359.

(12) *SADABS*: Area-Detector Absorption Correction; Siemens Industrial Automation, Inc.: Madison, WI, 1996.

(13) SIR97: Altomare, A.; Cascarano, G.; Giacovazzo, C.; Guagliardi, A.; Burla, M. C.; Polidori G.; Camalli, M. *J. Appl. Crystallogr.* **1994**, *27*, 435.

Table 3. Electrochemical Parameters for 2 and 4

complex	solvent	n_{app}[a]	D ($cm^2\ s^{-1}$)[a]	$v_{(n_{app}=1)}$[b] ($V\ s^{-1}$)	E_p[c] (V)	$E_p-E_{p/2}$[d] (mV)
2	THF	1.57 ± 0.16	6.3×10^{-6}	100	0.67	90
2	CH_2Cl_2	*e*	*e*	2	0.59	65
4	THF	1.95 ± 0.20	1.4×10^{-5}	50	1.04	90
4	CH_2Cl_2	*e*	*e*	1	0.99	68

[a] See Experimental Section and ref 11. [b] Values extracted from the normalized current functions of Figure 3. [c] Measured at 0.5 V s^{-1} vs SCE. [d] Constant values in the range of potential scan rate 2−200 V s^{-1} for **2** and 0.1−50 V s^{-1} for **4**. [e] Not measured.

all F^2.[14] Anisotropic displacement parameters were refined in both cases for all non hydrogen atoms, while hydrogen atoms were located from Fourier maps and refined isotropically. Final maps were featureless.

Simulations. Digital simulations of the voltammograms according to the proposed mechanism were performed with the program Antigona for applied electrochemistry (chronoamperometry and voltammetry) written by Loïc Mottier[15] and based on the Crank-Nicholson algorithm with a space exponential grid,[16] and with DigiSim (Bioanalytical Systems). The best simulation of the voltammograms of **2** were obtained by using the following set of parameters: $E_0^1 = 0.63$ V vs SCE, $k_0^1 = 0.15$ cm s^{-1}, $\alpha_1 = 0.5$, $E_0^2 = 0.28$ V vsSCE, $k_0^2 = 0.15$ cm s^{-1}, $\alpha_2 = 0.5$, $E_0^3 = 0.92$ vs SCE, $k_0^3 = 1.5 \times 10^{-2}$ cm s^{-1}, $\alpha_3 = 0.5$, $k_{1f} = 22\ s^{-1}$, $k_{1b} = 400\ s^{-1}$, $k_2 = 400\ s^{-1}$, and $k_3 = 0.6\ s^{-1}$.

Determination of the Absolute Electron Stoichiometry.[17] The chronoamperometric diffusion currents at 0.5 mm diameter gold disk electrode for a step duration of 0.2 s and the steady state currents at 12.5 μm radius gold microdisk electrode (potential scan rate 10 mV s^{-1}) were measured for 3 mM solutions of **2** and **4** and for the standard fluorenone [$D = (1.8 \pm 0.2) \times 10^{-5}\ cm^2\ s^{-1}$] under identical conditions, i.e., THF/0.2 M n-Bu_4NBF_4. These data allowed determination of the absolute consumption of electrons at the first oxidation wave of **2** and at the unique one of **4**, and their diffusion coefficients are reported in Table 3.

Results and Discussion

Synthesis and Structures. The new complexes [η^5-(1-ferrocenyl)indenyl]Rh(NBD) (**1**) and [η^5-(1-ferrocenyl)indenyl]Rh(COD) (**1a**) were synthesized by reacting $[Rh(\mu\text{-Cl})(NBD)]_2$[10a] and $[Rh(\mu\text{-Cl})(COD)]_2$,[10b] respectively, with (1-ferrocenyl)indenyllithium obtained by deprotonation of (3-ferrocenyl)indene (**3**)[3] in THF at low temperature. Column chromatography over activated basic Al_2O_3 afforded the products as orange microcrystalline powders in 80−87% yield. Complex **1** slowly crystallizes from cold *n*-pentane to give crystals suitable for single-crystal X-ray analysis; in contrast, no satisfactory crystals of **1a** were obtained.

The NMR spectra of **1** and **1a** are in accord with the proposed structures. For the sake of simplicity, the atom labeling of the complexes in the NMR discussion follows IUPAC convention. In particular, the four benzene ring protons give rise to an ABCD system and the H2 and H3 nuclei to an AX one. The coupling constant of H2 with ^{103}Rh amounts to 2 Hz, a value very close to that already reported for several η^5-indenyl-Rh(NBD) and η^5-indenyl-Rh(COD) complexes.[5f,i,j] The α,α' and β,β' protons of the indenyl-bonded Cp ring are slightly but definitely nonequivalent due to the chirality of the metal-coordinated (1-ferrocenyl)indenyl system (see below). In the ^{13}C spectrum the C1, C2, C3, C3a, and C7a carbon nuclei as well as the ferrocenyl quaternary C*j* and the NBD and COD olefin carbons couple with ^{103}Rh as already reported for other indenyl analogues.[5f,i,j]

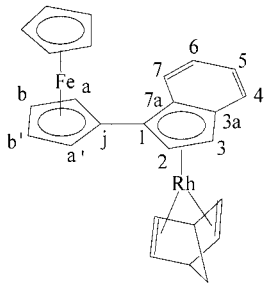

1

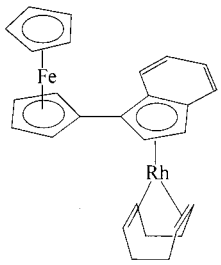

1a

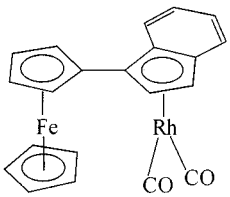

2

The new complex **2** was synthesized by bubbling CO at room temperature for 3 h through a slurry of **1** and *n*-pentane. The complex exhibits spectroscopic data in accord with the proposed chemical structure. In the ^{1}H NMR spectrum the coupling constant of H2 with ^{103}Rh was 2.6 Hz, a value very close to that already reported for other indenyl-Rh(CO)$_2$ complexes.[5i] In the ^{13}C spectrum the C1, C2, C3, C3a, and C7a carbon nuclei couple with ^{103}Rh as well as C*j*, and the CO's resonance appears at δ 190.4 with a $^1J(^{103}Rh-^{13}C) = 87$ Hz.

The molecular structures of **1**, **2**, and **3** are shown in Figure 1. Selected bond distances and bond angles are presented in Table 2.

The monometallic complex **3** might assume two nonequivalent configurations, a and b in Scheme 1, to avoid strong repulsive interactions between the *ortho* hydrogen atoms of the cyclopentadienyl ring and H7 and H11 of the indenyl ring.

The observed molecular structure corresponds to structure a, with the benzene ring oriented toward iron. It is achieved by a rotation of 25−26° of the indene plane about C4−C6. This structure seems to be slightly preferred owing to more relieved nonbonding interactions among hydrogen atoms, particularly those involving H7 or H11. For the same reasons the unsubstituted Cp ring of the ferrocene moiety is oriented in the eclipsed conformation. In a staggered conformation the hydrogen atoms H7 (or H11) would be at distances even shorter than 2.3−2.4 Å, as it can be demonstrated by using suitable molecular models.

In analogy with the corresponding diphenyl derivatives the rotation about C4−C6 is strongly prevented or greatly slowed; hence the indenyl ligand of this molecule may be regarded as a prochiral center. Thus,

(14) Sheldrick G. M. *SHELXL97, Program for structure refinement*; University of Goettingen: Germany, 1997.

(15) The program run under Windows 2000 and earlier versions and its running codes can be provided by Dr. L. Mottier; e-mail address: lmottier@libero.it.

(16) Speiser, B. In *Electroanalytical Chemistry, a Series of Advances*; Bard, A. J., Rubinstein, R., Eds.; Marcel Dekker: Basel, 1996; Vol. 19, p 1.

(17) Amatore, C.; Azzabi, M.; Calas, P.; Jutand, A.; Lefrou, C.; Rollin, Y. *J. Electroanal. Chem.* **1990**, *288*, 45.

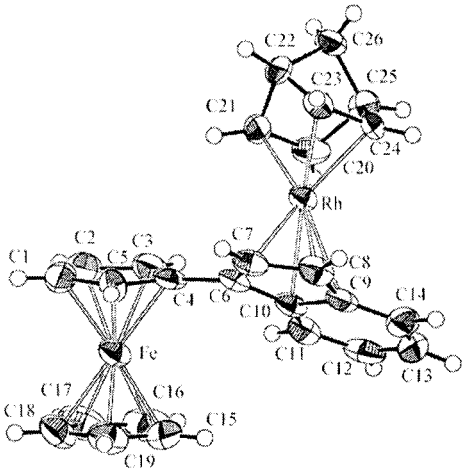

1

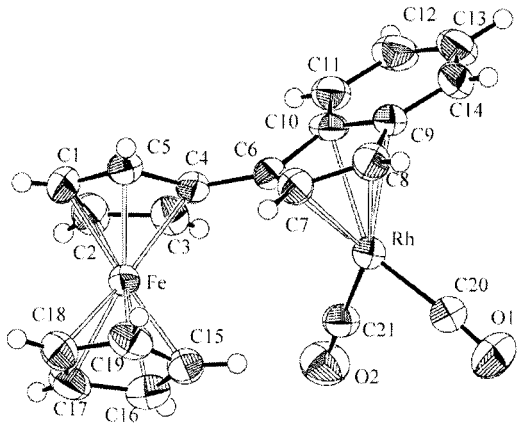

2

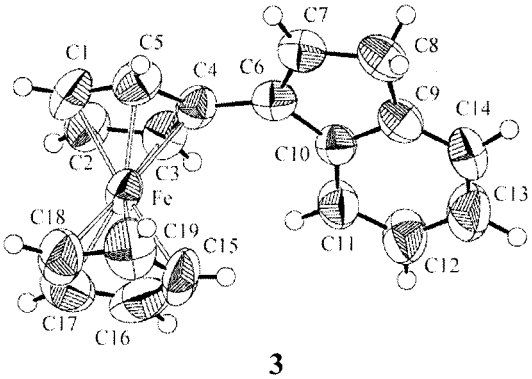

3

Figure 1. ORTEP views with thermal ellipsoids at 50% probability level of [η^5-(1-ferrocenyl)indenyl]Rh(NBD) (**1**); [η^5-(1-ferrocenyl)indenyl]Rh(CO)$_2$ (**2**); and (3-ferrocenyl)-indene (**3**).

the complexation with RhL_2 units on either of its two faces is not equivalent and gives rise to two distinct configurations and their correspondent *atropoisomers*.[18] It would be expected that an incoming RhL_2 would bind to the indenyl ring *transoid* to the ferrocenyl moiety,

(18) Hall. *Prog. Stereochem.* **1969**, *4*, 1−42. Öki. *Top. Stereochem.* **1983**, *14*, 1−81.

Scheme 1

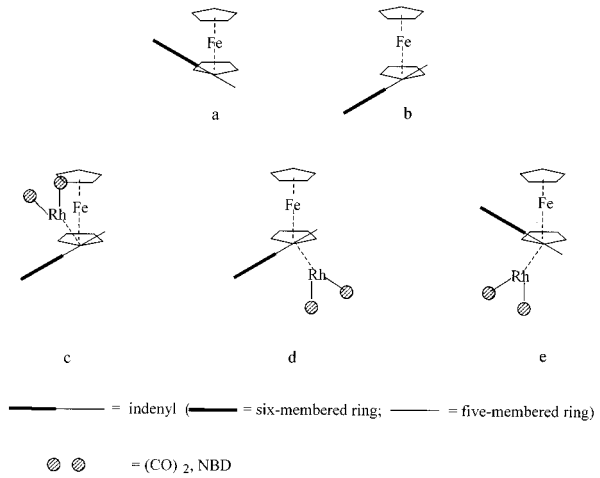

yielding conformation d or e in Scheme 1. Such an arrangement would maximize the distances between the L groups and the cyclopentadienyl rings.

Interestingly, the observed molecular structure of **2** (L = CO) shows the unexpected features of conformation c. In this structure, the orientation of the indenyl group corresponds to the less favorable conformation b of Scheme 1, and the $Rh(CO)_2$ group is coordinated in the *cisoid* arrangement with respect to the ferrocene group. This configuration gives rise to short intramolecular contact distances, e.g., H15···C21 (2.85 Å) and H16···O2 (2.95 Å). In other complexes[19] these distances have been attributed to weak π-hydrogen bond interactions. We believe that the present structure of **2** is actually controlled by these stabilizing interactions and exclude any prevailing influence of packing effects.

The observed molecular structure of **1** can be assumed as a further confirmation of this hypothesis. In this complex the attack of the Rh(NBD) group occurs, as above predicted, according to e in Scheme 1. We believe that the *cisoid* conformation is severely hampered by stereochemical reasons, not only by the larger bulkiness of the NBD group but presumably also by the impossibility to establish any stabilizing interaction of π-hydrogen bond type.

The geometrical parameters of the (1-ferrocenyl)-indenyl residue are quite similar for the three complexes. The bond lengths are in ranges typical for comparable resonant systems. The iron is coordinated η^5 to both the cyclopentadienyl rings with distances in the range 2.03−2.04 Å. The five-membered rings lie in planes almost parallel and are always arranged eclipsed to each other, as explained above, with a twist angle between them not larger than 3−8°. The torsion angle C3−C4−C6−C10 is 25.2° for **3**, −52.7° for **2**, but again 27.0° for **1**, confirming that the more favorable conformation of the ferrocenyl-indenyl residue is that shown in Scheme 1a. It is worth noting that the orientations of the $Rh(CO)_2$ group in **2** and of the Rh(NBD) group in **1** with respect to the indenyl moiety are such that they maintain a C_s local pseudo-symmetry as usually found

(19) (a) Stainer, T.; Tamm, M.; Lutz, B.; van der Maas, J. *J. Chem. Soc., Chem. Commun.* **1996**, 1127. (b) Bitterwolf, T. E.; Ceccon, A.; Gambaro, A.; Ganis, P.; Kuck, D.; Manoli, F.; Rheingold, A. L.; Valle, G.; Venzo, A. *J. Chem. Soc., Perkins Trans. 2* **1997**, *2*, 735. (c) Ceccon, A.; Gambaro, A.; Manoli, F.; Ganis, P.; Kuck, D.; Bitterwolf, T. E.; Valle, G.; Venzo, A. *J. Chem. Soc., Perkins Trans. 2* **1991**, *2*, 233.

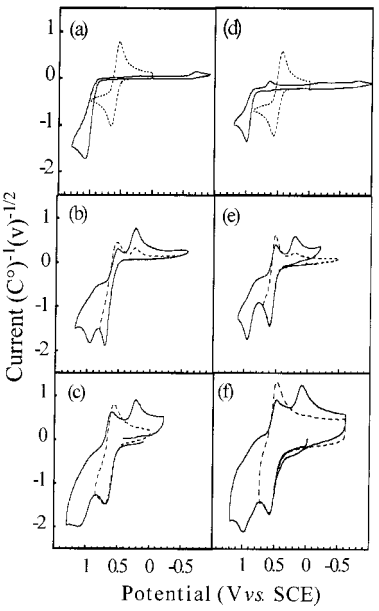

Figure 2. Cyclic voltammetric scan at a gold disk electrode (diameter 0.5 mm, $0.05 \le v \le 0.5$, and 0.125 mm, $1 \le v \le 200$), $T = 20$ °C. The current is normalized by $v^{1/2}$ M^{-1}. Solvent THF/0.2 M *n*-Bu_4NBF_4: (a) solid line 3 mM η^5-indenyl-Rh$(CO)_2$ (**4**), dashed line 3 mM ferrocene, $v = 0.5$ V s^{-1}; (b) solid line 3 mM [η^5-(1-ferrocenyl)indenyl]-Rh$(CO)_2$ (**2**), dashed line 3 mM **2** with the scan inverted after the first wave at 0.83 V, $v = 0.5$ V s^{-1}; (c) solid line 3 mM **2**, dashed line 3 mM **2** with the scan inverted after the first wave at −0.85 V, $v = 100$ V s^{-1}. Solvent CH_2Cl_2/0.2 M *n*-Bu_4NBF_4: (d) solid line 3 mM **4**, dashed line 3 mM ferrocene, $v = 0.5$ V s^{-1}; (e) solid line 3 mM **2**, dashed line 3 mM **2** with the potential scan inverted after the first wave at −0.70 V, $v = 0.5$ V s^{-1}; (f) solid line 3 mM **2**, dashed line 3 mM **2** with the potential scan inverted after the first wave at −0.73 V, $v = 100$ V s^{-1}.

in many similar structurally characterized compounds.[5h,k,20]

Electrochemical Oxidation of Monometallic Compounds. For the sake of comparison, we report first the voltammetric behavior of the mononuclear (3-ferrocenyl)indene (**3**) and η^5-indenyl-Rh$(CO)_2$ (**4**) in THF/0.2 M *n*-Bu_4NBF_4.

The voltammetric oxidation of **3** occurs as a one-electron reversible process over all the potential scan rates investigated ($v = 0.05-50$ V s^{-1}) with $E_{1/2}$ and $\Delta E_p = E_{pa} - E_{pc}$ values (0.57 V and 80 mV) practically identical to those found for ferrocene under the same conditions (0.56 V and 74 mV, see Figure 2a for a CV scan of ferrocene).

On the contrary, the voltammetric oxidation of **4** displays a chemically irreversible wave (Figure 2a) ($E_p = 1.08$ at $v = 0.5$ V s^{-1}) in the range of potential scan rate 0.05−200 V s^{-1}. The peak current of the oxidation wave (Figure 3a) is not proportional to $v^{1/2}$ as would be expected for a simple reversible process.[21a] The current function, $i_p v^{-1/2}$, decreases upon increasing the potential scan rate and reaches a constant value for v between 50 and 200 V s^{-1}. In this range the plot of E_p vs the potential scan rate displays a slope $d(E_p)/d(\log v) = 53$ mV (Figure 3b), which allows an estimate of the value of the coefficient of the electron transfer $\alpha = 0.55$ (T 20 °C) from eq 1 describing the variation of the peak potential for a totally irreversible electron transfer ($n_\alpha = 1$):[21b]

$$E_p = (1.15RT/\alpha n_\alpha F)\log v + \text{constant} \qquad (1)$$

In the general case in which the electron transfer is nernstian at low scan rate and irreversible at high scan rate the current function normalized to its value at the highest scan rate is expected to reach the maximum

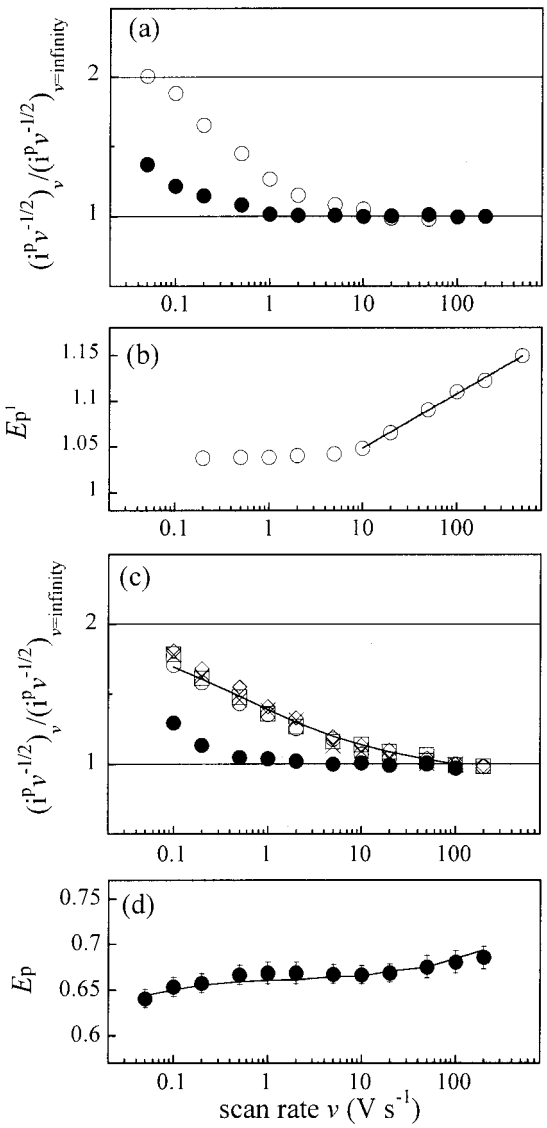

Figure 3. Variations of the current function $i_p v^{-1/2}$ M^{-1} normalized to its value at high scan rate $v \ge 100$ V s^{-1} and of the peak potential E_p of the (first) oxidation wave at a gold disk electrode (0.5 and 0.125 mm diameter according to the scan rate), $T = 20$ °C. Abscises in logarithmic scale. Symbols: experimental data; solid lines: theoretical variation based on the simulation results. (a) 3 mM η^5-indenyl-Rh$(CO)_2$ (**4**) in THF/0.2 M *n*-Bu_4NBF_4 (empty circles) and in CH_2Cl_2/0.2 M *n*-Bu_4NBF_4 (full circles); (b) 3 mM **4** in THF/0.2 M *n*-Bu_4NBF_4; (c) 2 mM (open circles), 4 mM (open square), 6 mM (open diamonds), and 8 mM (crosses) [η^5-(1-ferrocenyl)indenyl]Rh$(CO)_2$ (**2**) in THF/0.2 M *n*-Bu_4NBF_4 and 3 mM in CH_2Cl_2/0.2 M *n*-Bu_4NBF_4 (full circles); (d) 3 mM **2** in THF/0.2 M *n*-Bu_4NBF_4.

(20) Kakkar, A. K.; Jones, S. F.; Taylor, N. J.; Collins, S.; Marder, T. B. *J. Chem. Soc., Chem. Commun.* **1989**, 1454.
(21) (a) Bard, J.; Faulkner, L. F. *Electrochemical Methods*, 2nd ed.; Wiley: New York, 2001; p 230; (b) p 236; (c) p 473.

factor of $0.446/0.495(\alpha)^{1/2}$.[21a,b] In the case of complex **4** the calculated factor is 1.2, much lower than the observed one, i.e. 2.0, indicating that the kinetics of the electron transfer alone does not justify the variation of the current function.

These data together with the determination of the absolute electron stoichiometry[17] at sufficiently low scan rate (Table 3, $n_{app} = 1.95$ at $v \leq 0.1$ V s^{-1}) indicate that at sufficiently low scan rate the oxidation of **4** is a two-electron process and it becomes a single-electron process at high scan as expected for an E_1CE_2 mechanism with $E_0^1 \geq E_0^2$ (eqs 2−4). The oxidation is followed by the appearance of a cathodic wave at $E_p = -0.66$ (Figure 2a, $v = 0.5$ V s^{-1}) on the reverse scan of the potential, which arises from reduction of an oxidation product. Finally, the oxidation in CH_2Cl_2 (DN = 0)[22] shows a CV similar to that in THF (Figure 2d), but the peak current function $i_p v^{-1/2}$ decreases to one at lower scan rate (Figure 3a), indicating that the oxidation is of single-electron nature at 1 V s^{-1}. This behavior suggests a crucial role for the strongly coordinating THF (DN = 20.0)[22] in the overall electrode reaction. From the comparison of the results in the two solvents the chemical step seems to be the coordination of one solvent molecule to the 17-electron radical cation (eq 3) yielding the corresponding 19-electron radical cation. This oxidizes to the corresponding 18-electron dication at less positive potential (eq 4), the chemical step being faster when the solvent is THF, as expected.[23]

$$\underset{18\ e}{\eta^5\text{-indenyl-Rh(CO)}_2} \overset{E_1}{\rightleftharpoons} \underset{17\ e}{[\eta^5\text{-indenyl-Rh(CO)}_2]^{+\bullet}} + e^- \quad (2)$$

$$\underset{17\ e}{[\eta^5\text{-indenyl-Rh(CO)}_2]^{+\bullet}} \xrightarrow[\text{THF}]{C} \underset{19\ e}{[\eta^5\text{-indenyl-Rh(CO)}_2]^{+\bullet}} \quad (3)$$

$$\underset{19\ e}{[\eta^5\text{-indenyl-Rh(CO)}_2]^{+\bullet}} \overset{E_2}{\rightleftharpoons} \underset{18\ e}{[\eta^5\text{-indenyl-Rh(CO)}_2]^{2+}} + e^- \quad (4)$$

Electrochemical Oxidation of the Bimetallic Compound 2. The molecular structure of **2** can be formally regarded as an assembly of the two monometallic fragments ferrocene and η^5-indenyl-Rh(CO)$_2$. The comparison between CVs of ferrocene and **4** at $v = 0.5$ V s^{-1} (see Figure 2a) shows that the rhodium complex oxidizes at a potential more positive by about 550 mV than ferrocene. An equimolar mixture of these two complexes did not point out any interaction upon oxidation. Cyclic voltammograms of **2** in THF/0.2 M n-Bu$_4$NBF$_4$ at different scan rates are illustrated in Figure 2b,c. The voltammetric scan at 0.5 V s^{-1} (Figure 2b) shows two anodic waves, $E_p^1 = 0.68$ and $E_p^2 = 0.95$ V vs SCE, the first being of limited chemical reversibility, the second being irreversible in the chemical sense. After inversion of the scan a reduction wave appears at $E_p = 0.24$ V, whose size depends on the potential of the scan reversal; that is, it decreases when the first oxidation wave is the only one traversed. However, if the potential is maintained at 0.67 V for a few seconds, the size of the reduction wave is reestablished. This evidence indicates that this reduction wave arises from a chemical step occurring as a result of the first oxidation. The fact that it appears even if the second oxidation wave is scanned could be interpreted only in terms of allowing more time for **2** to undergo oxidation and subsequent chemical reaction at the first wave. Nevertheless we cannot exclude a further contribution arising from the second oxidation (see below the discussion for high scan rate results and digital simulation). As shown in Figure 2c, at $v > 50$ V s^{-1} the first wave becomes electrochemically reversible, $E_{1/2}^1 = 0.64$ V, $\Delta E_p = E_{pa}^1 - E_{pc}^1 \simeq 80$ mV, as expected for a nernstian electron transfer in the low conductive solvent THF.[19] Moreover, the first wave becomes chemically reversible ($i_{pa}/i_{pc} \approx 1$). This behavior indicates that the first wave is not controlled by the kinetics of the electron transfer. The peak current functions ($i_p v^{-1/2}$ M^{-1}) of the first and second waves were not constant with scan rate. Figure 3c shows the variation of this current function at different concentrations of the substrate (normalized to its value at high scan rate). This normalized current function decreases by increasing the scan rate, indicating that the first oxidation involves a subsequent reaction coupled with further oxidation at lower potential (EC mechanism).[21c] At the same time, the second wave decreases to almost zero at low scan rate. Determination of the absolute electron stoichiometry[17] at sufficiently low scan rate ($n_{app} = 1.57$ at $v \leq 0.1$ V s^{-1}, Table 3) confirmed that at this time scale (0.2 s) the first oxidation wave tends to be bielectronic while the second one tends to vanish. The situation is well depicted by the steady-state voltammogram at a 12.5 μm radius microdisk electrode (Figure 4) in which the ratio between the two anodic *plateau*'s ($i_{lim}^2/i_{lim}^1 = 0.41/1.59$) is in remarkable agreement with the current function at the same time scale.[24]

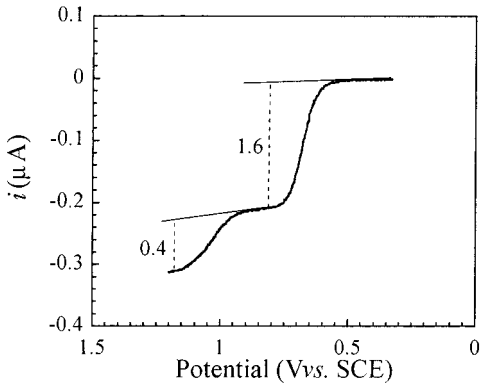

Figure 4. Steady-state cyclic voltammogram of 3 mM [η^5-(1-ferrocenyl)indenyl]Rh(CO)$_2$ (**2**) in THF/0.2 M n-Bu$_4$NBF$_4$ at a gold microdisk electrode, $r = 12.5$ μm, $v = 5$ mV s^{-1}.

The behavior at 100 V s^{-1} is depicted by the CV in Figure 2c. The relative current height of the second oxidation wave with respect to that of the first wave is

(22) Gutmann, V. *The Donor−Acceptor Approach to Molecular Interactions*, Plenum Press: New York, 1978.
(23) Kukharenko, S. V.; Strelets, V. V.; Kudinov, A. R.; Kreidlin, A. Z.; Petrleitner, M. G.; Denisovich, L. I.; Rybynskaya, M. I. *J. Organomet. Chem.* **1996**, *519*, 1.

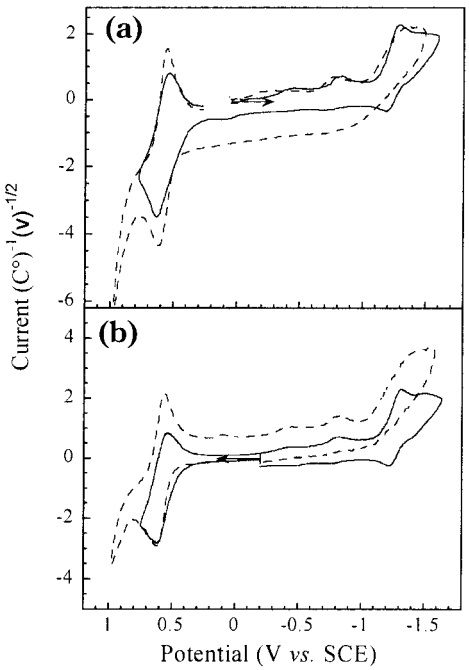

Figure 5. (a) Voltammetric reduction and (b) voltammetric oxidation of 6 mM [η^5-(1-ferrocenyl)indenyl]Rh(CO)$_2$]$^{2+}$ (**2c**$^{2+}$) in THF/0.2 M *n*-Bu$_4$NBF$_4$ at a gold disk electrode 0.5 mm diameter, $v = 0.5$ V s^{-1}, $T = 20$ °C obtained after 2 faraday per mole electrolytic oxidation of **2** (dotted line) after chemical oxidation of **2** with 2 equiv of *p*-benzoquinone in THF (solid line).

considerably larger at this scan rate relative to that observed at lower scan rates. The CV corresponds to two one-electron oxidation processes. Within experimental error no concentration dependence of the current function was observed.

Preparative scale electrolytic oxidation of **2** at 0.59 V, 60 mV negative of the peak potential of the first wave, requires 2 faraday per mole. The final CVs show one reversible anodic wave with the typical values of the ferrocene system under the same conditions, $E_{1/2} = 0.58$ V and $\Delta E_p = E_{pa} - E_{pc} = 80$ mV in THF (Figure 5a), and one irreversible cathodic wave at $E_p = -1.35$ V (Figure 5b).

The behavior of the first wave is characteristic of an $EC_{rev}E$ mechanism:[25]

$$\mathbf{2} \rightleftharpoons \mathbf{2a}^+ + e^- \qquad (E_p{}^1 = 0.68 \text{ V vs SCE}) \qquad (5)$$

$$\mathbf{2a}^+ \rightleftharpoons \mathbf{2b}^+ \qquad k_{1f},\ k_{1b}\ (v \le 50 \text{ V s}^{-1}) \qquad (6)$$

$$\mathbf{2b}^+ \rightleftharpoons \mathbf{2b}^{2+} + e^- \qquad (E_p{}^2 \le E_p{}^1) \qquad (7)$$

The iron-centered radical cation **2a**$^+$ formed after the first electron transfer (eq 5) undergoes a reversible chemical transformation (eq 6) leading to a product **2b**$^+$, which oxidizes to **2b**$^{2+}$ at lower potential (eq 7), as discussed below. The cathodic wave at $E_0{}^2 = 0.28$ V corresponds to the reduction process (**2b**$^{2+}$/**2b**$^+$). At high scan rates the chemical step is frozen and the process results in two one-electron oxidations, the first (**2**/**2a**$^+$) iron-centered (equation 5), the second (**2a**$^+$/**2a**$^{2+}$) rhodium-centered (eq 8).

$$\mathbf{2a}^+ \rightleftharpoons \mathbf{2a}^{2+} + e^- \qquad (E_p{}^3 = 0.97 \text{ V vs SCE}) \qquad (8)$$

$$\mathbf{2a}^{2+} \rightarrow \mathbf{2b}^{2+} \qquad k_2\ (v \ge 500 \text{ V s}^{-1}) \qquad (9)$$

The existence of the chemical step (eq 9) is supported by the appearance of the cathodic wave at $E_0{}^2 = 0.28$ V even at high rate when the potential is reversed after the second wave (Figure 2c). This evidence indicates that the cathodic wave comes from the reduction of the intermediates formed at the potential of both the oxidation waves. This means that the dication **2b**$^{2+}$ is produced through the two different pathways of Scheme 2. On the other hand, the absence of the expected reversibility of the cathodic wave even at the highest scan rate used (500 V s^{-1}) is due to the presence of the back reaction of eq 6, which is faster than the forward step, as expected on thermodynamic grounds. In fact, the electron-withdrawing ligand CO destabilizes the positive charge on the rhodium center favoring the corresponding cation **2a**$^+$. The slowing down of the chemical process in the less coordinating solvent CH_2Cl_2 is clear evidence of the role of the solvent in stabilizing **2b**$^{2+}$ in analogy with that found for the monometallic complex **4** (Figure 3a). In fact, the peak current function of the first wave, $i_p v^{-1/2}$, reaches the value of 1 at lower scan rate ($v = 0.5$ V s^{-1}, Figure 2c), and the corresponding CV (Figure 2e) shows the same behavior as that in THF at 100 V s^{-1} ($E_{1/2}{}^1 = 0.55$ V, $\Delta E_p = E_{pa}{}^1 - E_{pc}{}^1 = 80$ mV; $E_p{}^2 = 0.95$ V). For the sake of completeness, in Figure 2f we show the CV in CH_2Cl_2 at 100 V s^{-1}. The results of digital simulation are in agreement with the proposed mechanism (see section below).

The easier oxidation of **2b**$^+$ with respect to **2** is explained by the existence of a strong interaction between the two metals favored by their proximity in the more stable *cisoid* configuration. As a consequence, an internal electron transfer from Rh to Fe takes place with incipient formation of a metal−metal bond and concomitant with a strong rearrangement of the ligand from a planar to a bent fulvalenyl frame. This results in the reduction from Fe(III) to Fe(II), which further oxidizes at a less positive potential. Analogous internal electron transfer was found, for instance, in the reduction of *anti*- and *syn*-{Cr(CO)$_3$-(μ:η,η-indenyl-Rh(COD)} complexes[25] and in the oxidation of [η^5-(1-ferrocenyl)-cyclopentadienyl-Cr(CO)$_3$].[26] A bent fulvalenyl frame was proposed for homobimetallic complexes of different transition metals.[27]

Chemical Oxidation of Bimetallic Complex 2. Reaction of **2** with 2 equiv of *p*-benzoquinone in THF yields a brown powder, which exhibits the same voltammogram obtained after 2 faraday per mole electrolysis of **2** (Figure 5).

(24) The characteristic time T_c for a steady-state cyclic voltammogram at the microdisk electrode is a function of the electrode radius r and diffusion coefficient D of the substrate, $T_c = r^2/D$. In the present case ($r = 1.25 \times 10^{-3}$ cm and $D = 6.3 \times 10^{-6}$ cm^2 s^{-1}) T_c is 0.25 s, corresponding approximately to a scan rate of 0.1 V s^{-1} ($v \approx RT/FT_c$) in transient cyclic voltammetry.

(25) Amatore, C.; Ceccon, A.; Santi, S.; Verpeaux, J. N. *Chem. Eur. J.* **1999**, *5*, 3357.

(26) Yeung, L. K.; Kim J. E.; Chung, Y. K.; Rieger, P. H.; Sweigart, D. A. *Organometallics* **1996**, *15*, 3891.

(27) Moulton, R. D.; Weidman, T. W.; Vollhardt, K. P. C.; Bard, A. J. *Inorg. Chem.* **1986**, *25*, 1846.

Scheme 2

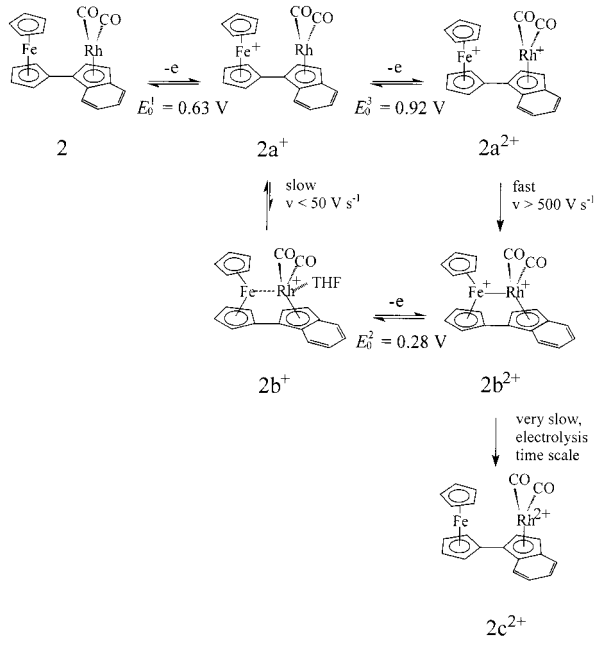

The IR spectrum in CH_2Cl_2 shows two ν_{CO} bands at 2097 and 1922 cm^{-1} which are shifted 60 cm^{-1} to higher frequency than those of the neutral complex **2**, as expected for the presence of positive charge on a metal carbonyl group.[28] The NMR spectrum of this species is consistent with a diamagnetic species and exhibits the characteristic signals of the [η^5-(1-ferrocenyl)indenyl]-RhL_2 system (see Experimental Section); noteworthy differences are the upfield shift of the resonances of carbon atoms C3a and C7a ($\Delta\delta^{13}C = -10$ ppm) and the increase of the Rh−C3a and Rh−C7a coupling constants, diagnostic of a more marked η^5 hapticity of indenyl, and of CO's ($\Delta\delta^{13}C = -16$ ppm), in agreement with the effect of a positive charge on metal carbonyl derivatives.[29]

On the basis of these spectroscopic characteristics and of the voltammetric behavior, we infer that this species is the dication **2c**$^{2+}$ (see Scheme 2), containing a neutral ferrocene unit and a dicationic indenyl-$Rh(CO)_2$ unit. We suggest that, on the time scale of preparative oxidation, **2c**$^{2+}$ can be formed by the rearrangement of the dication **2b**$^{2+}$ through a further internal electron transfer from rhodium to iron and cleavage of the metal−metal interaction.

Oxidation Mechanism of 2 Using Digital Simulation. The mechanism shown in Scheme 2 is qualitatively proposed on the basis of cyclic voltammetry at different scan rates and preparative scale electrolysis. Its assessment on quantitative grounds requires the use of digital simulation because of the multiplicity of the heterogeneous and homogeneous rate constants. The search of the fitting set of parameters must be pursued step by step: first of all the electrochemical parameters E_0^1, α_1, and $k_1°$ of the first oxidation wave were determined; E_0^2, α_2, $k_2°$, E_0^3, α_3, $k_3°$, and the rate constant of the follow-up reactions were introduced one at a time in a second stage.[25,30]

The experimental voltammograms at high potential scan rate ($v \geq 50$ V s^{-1}), that is, when the oxidation process is limited to the first electron transfer **2a**/**2a**$^+$ without interference of any homogeneous reaction, indicate that the process is nernstian and the value $\alpha_1 = 0.5$ was used in the simulation. The standard potential ($E_0^1 = 0.63$ V) and the heterogeneous rate constant ($k_1° = 0.15$ cm s^{-1}) were adjusted from the peak potential position of the wave in the same range of scan rate.

The parameters E_0^2, α_2, and $k_2°$ relative to the second electron transfer can be obtained from the reverse reduction wave using the voltammograms at low scan rate in the range 0.1−5 V s^{-1} when this wave actually corresponds to the process **2b**$^{2+}$/**2b**$^+$. The shift of the peak potential is 30 mV per decade of log v, indicating that also the second electron transfer is nernstian and $\alpha_2 = 0.5$ was set. The standard potential ($E_0^2 = 0.28$ V) and the heterogeneous rate constant ($k_2° = 0.15$ cm s^{-1}) were also adjusted from the peak potential position.

The parameters of the second oxidation wave related to the redox couple **2a**$^+$/**2a**$^{2+}$ were similarly extracted from the voltammograms at high scan rate in the range 50−200 V s^{-1}, the wave being still chemically irreversible. The experimental peak potential shift $d(E_p^3)/d(\log v) = 58$ mV corresponds to $\alpha_3 = 0.52$; the standard potential $E_0^3 = 0.92$ and $k_3° = 1.5 \times 10^{-2}$ cm s^{-1} were optimized from the peak potential position, too.

While the position of the oxidation waves is essentially governed by the standard potentials and the heterogeneous rate constants of the electron transfer, the current primarily depends on the kinetics of the homogeneous reactions. The variation from two to one electron of the first oxidation wave and from almost zero to one electron of the second one reflects the presence of a dynamic equilibrium between **2a**$^+$ and **2b**$^+$ ($K = k_{1f}/k_{1b}$) which controls (i) the second electron transfer of the $EC_{rev}E$ mechanism (Scheme 2) and (ii) the intensity of the second oxidation wave. In the mechanism proposed the current of the first peak depends mainly on the kinetic parameter $(k_{1f})^2/k_{1b}$, which governs[31] the possibility of regenerating the form **2a**$^+$ through a backward displacement of the equilibrium at the oxidation potential of **2**. First, this parameter was varied in order to fit the experimental peak current function of the first oxidation wave (Figure 3c). In particular, k_{1f} was optimized from the peak current of the anodic wave in the range of higher scan rates ($v \geq 1$ V s^{-1}), and then k_{1b} was adjusted from the same peak current in the range of lower scan rates. Afterward, a slight variation of k_{1f} and k_{1b} at low scan rates allowed the relative intensity of the second anodic wave to be optimized. The best fitting was obtained with $(k_{1f})^2/k_{1b} = 1.21$. At the highest scan rate investigated, 500 V s^{-1}, the irreversibility of the second electron transfer ($E_0^2 = 0.28$ V) was satisfied by the individual values $k_{1f} = 22$ s^{-1} and $k_{1b} = 400$ s^{-1}, which represent the minimum

(28) (a) Cotton, F. A.; Wilkinson, J. *Advanced Inorganic Chemistry*, 3rd ed.; Wiley-Interscience, New York, 1972; Chapter 22. (b) Graham, P. B.; Rausch, M., D.; Täskler, K.; von Philipsborn, W. *Organometallics* **1991**, *10*, 3049.

(29) (a) Acampora, A.; Ceccon, A.; Dal Farra, M.; Giacometti, G.; Rigatti, G. *J. Chem. Soc., Perkin Trams. 2* **1977**, 483. (b) Ceccon, A.; Gambaro, A.; Agostini, G.; Venzo, A. *J. Organomet. Chem.* **1981**, *217*, 79, and references therein.

(30) Amatore, C.; Ceccon, A.; Santi, S.; Verpeaux, J. N. *Chem. Eur. J.* **1997**, *3*, 279.

(31) (a) Amatore, C.; Jutand, A.; Medeiros, M. J., Mottier, L. *J. Electroanal. Chem.* **1997**, *422*, 125. (b) Amatore, C.; Savéant, J. M. *J. Electroanal. Chem.* **1977**, *85*, 27. (c) Amatore, C.; Savéant, J. M. *J. Electroanal. Chem.* **1980**, *107*, 353.

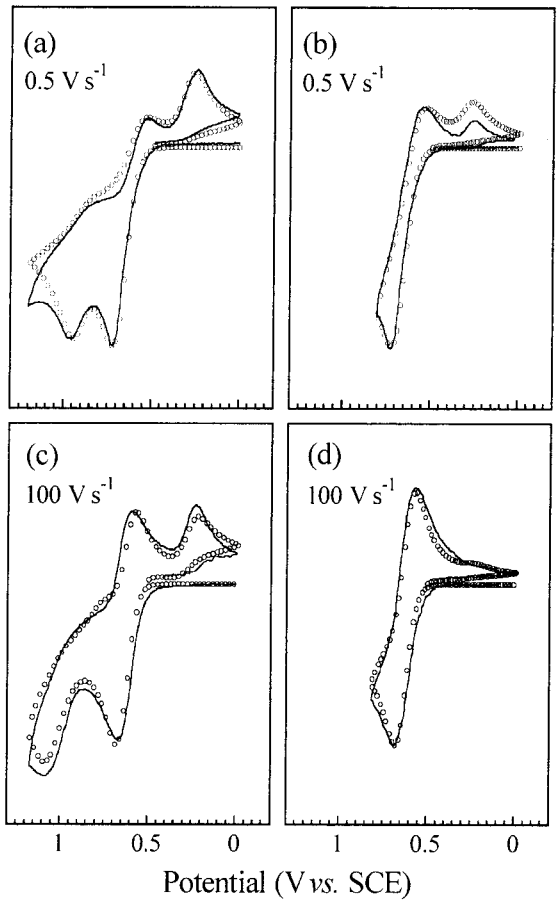

Figure 6. Experimental (solid line) and simulated (open circles) voltammetric oxidation of [η^5-(1-ferrocenyl)indenyl]-$Rh(CO)_2$ (**2**) in THF/0.2 M *n*-Bu_4NBF_4 at a gold disk electrode 0.5 mm diameter, $T = 20$ °C: (a) $v = 0.5$ V s^{-1}; (b) at $v = 0.5$ V s^{-1}, potential scan inverted after the first wave; (c) $v = 100$ V s^{-1}; and (d) at $v = 100$ V s^{-1}, potential scan inverted after the first wave.

values of the true rate constants.[32] Finally, the partial reversibility of the first oxidation wave, the irreversibility of the second oxidation wave, and the intensity at high scan rate of the reduction wave with $E_0^2 = 0.28$ V were set by introducing two consecutive irreversible chemical reactions (eqs 9 and 10) into the digital simulation with rate constants k_2 and k_3, respectively:

$$\mathbf{2a}^{2+} \rightarrow \mathbf{2b}^{2+} \qquad k_2\ (v > 500\ \text{V s}^{-1}) \qquad (9)$$

$$\mathbf{2b}^{2+} \rightarrow \mathbf{2c}^{2+} \qquad k_3\ (v < 0.5\ \text{V s}^{-1}) \qquad (10)$$

The former reaction with constant $k_2 > 400$ s^{-1} accounts for the experimental chemical irreversibility of the second anodic wave at the overall scan rate investigated; however, it makes totally chemically irreversible the first wave and too much intense the reduction wave at $E_0^2 = 0.28$ V. The partial reversibility of the first wave observed at low scan rate and the correct intensity of the reduction wave are well reproduced by introducing the last reaction with rate constant $k_3 = 0.6$ s^{-1}.

This simulation procedure allowed us to find a basic set of thermodynamic and kinetic parameters. Variation (≤10%) of each parameter enables reproduction of the voltammetric behavior over the whole range of the potential scan rate investigated. The good agreement between the experimental and calculated voltammograms is shown in Figure 6 as well as the agreement between the measured electrochemical parameters (E_p and $i_p v^{-1/2}$) and their simulated variations (Figure 3c,d).

Conclusions

In the present paper the synthesis of the title bimetallic complexes in which the two metals, iron and rhodium, are coordinated to the fulvalenyl frame was successful. The crystallographic analysis showed that the metal units are in two different configurations depending on the nature of the ancillary ligands, i.e., *cisoid* with L = CO and *transoid* with L_2 = NBD.

The electrochemical studies revealed a strong metal−metal interaction in the carbonylated derivative favored by the relative proximity of the metal groups in the ground state configuration. The oxidation proceeds through a route in which the iron works as a sink of electrons supplied by rhodium with the consequence that the oxidative activation of rhodium mediated by the ferrocenyl group is possible at a potential far lower than that required for direct oxidation of the metal. We suggest that the driving force is the internal electron transfer from rhodium to iron concomitant with the rearrangement of the bridging ligand from a planar to a bent fulvalenyl frame and formation of a metal−metal dative bond.

Acknowledgment. This work was supported by the Ministero dell'Università e della Ricerca Scientifica e Tecnologica MURST (COFIN 99, Project code 9903198953), by the Progetto SolvET of Università di Padova, and by the CNR (Roma) through its Centro di Studi sugli Stati Molecolari, Radicalici ed Eccitati (Padova).

Supporting Information Available: Final positional and thermal parameters, and complete list of the geometrical parameters for **1**, **2**, and **3**. This material is available free of charge via the Internet at http://pubs.acs.org.

OM010621G

(32) The values of the rate constants k_{1f}, k_{1b}, and k_2 represent the minimum values of the true rate constants since the experimental conditions (capacitive current, waves controlled by the kinetics of the electron transfer at scan rate higher than 500 V s^{-1} for electrochemical step E_2 and E_3) failed to verify the reversibility (if any) of the second anodic wave and of the cathodic wave at $E_0^2 = 0.28$ V.